$3p$ photoabsorption of free and bound Cr, Cr$^+$, Mn, and Mn$^+$

J. T. Costello and E. T. Kennedy
Dublin City University, Glasnevin, Dublin 9, Ireland

B. F. Sonntag
II Institute für Experimentalphysik, Universität Hamburg, Hamburg, West Germany

C. W. Clark
National Institute of Standards and Technology, Gaithersburg, Maryland 20899
(Received 16 July 1990)

A dual-laser-plasma technique has been used to measure photoabsorption by atomic Cr and Mn and their ions at photon energies between 40 and 70 eV, where the dominant absorption mechanism is excitation of the $3p$ subshell. No dramatic differences are observed between the absorption spectra of Mn and Mn$^+$, and these spectra are similar to those of Mn metal and MnCl$_2$. The spectra of Cr and Cr$^+$ are strikingly dissimilar, the mean excitation energy being about 5 eV greater in the ion. We attribute this to strong mixing of the localized $3d^6$ configuration with $3d^5nd$ Rydberg configurations, an effect that is also responsible for the anomalous appearance of the Cr spectrum with respect to those of the other iron-period elements. The absorption spectra of Cr metal and CrCl$_2$ take forms intermediate between those of Cr and Cr$^+$. We give spectroscopic assignments to most of the sharp absorption features of Cr$^+$ and determine the $3p$ ionization thresholds from quantum-defect analysis.

INTRODUCTION

The measurement of photoionization cross sections of free ions is difficult, as a suitable absorbing column must be produced and backlighted by a bright, synchronized extreme-ultraviolet (EUV)-continuum emitting source. It is important, however, that reliable and versatile experimental techniques are developed, as photoabsorption experiments provide valuable information on many-electron effects in atoms and ions. This is particularly the case when changes in behavior along isoelectronic sequences are studied. The results of such experiments are important for a comparison with theory,[1-9] and the cross-sectional data are of interest to plasma physicists and astrophysicists.[10,11] Systematic studies of the differences between the photoionization of free atoms and that of the corresponding atoms or ions in molecular and/or solid complexes can lead to a better understanding of solid-state effects.[12-17]

A number of different experimental techniques have been explored to date. Flash pyrolysis has, for example, been used by Parkinson and co-workers[18] to study the EUV photoabsorption of neutral and singly ionized lithium. Esteva and Mehlman[19,20] used BRV devices to produce both absorbing and back-lighting plasmas and studied photoabsorption in Be I and Be II and Mg I and Mg II. More recently, West and collaborators[21,22] carried out photoionization cross-section measurements of ions by using ion beams in conjunction with synchrotron radiation. A major advantage of this technique is that it allows absolute cross sections to be determined. Results have been obtained for K$^+$, Ca$^+$, Sr$^+$, and Ba$^+$ and compared with calculated cross sections.

In the present work, both resonant laser-driven ionization and dual laser plasma techniques have been utilized. In resonant laser-driven ionization (RLDI) the absorbing-ion column is created by the interaction of a dye laser beam (tuned to a resonance transition), with the corresponding atomic vapor produced in a heat pipe. Doubly ionized species can be produced by the subsequent irradiation of the singly ionized column by a second, time-delayed dye laser beam. Resonant laser-driven ionization was first used by Lucatorto and McIlrath[23] to study the photoabsorption of singly ionized sodium in the 23–33-eV region. Subsequently, Li*, Li$^+$, Cs$^+$, Ca, Ca*, and Ca$^+$ spectra have been obtained in a series of experiments.[24-27] The power of the technique was illustrated by the study of the isonuclear sequence Ba, Ba$^+$, and Ba^{2+}, which provided considerable insight[28-30] into the collapse of the $4f$ wave function as the degree of ionization increased, leading to an increase in the overlap between $4d$ and nf orbitals with larger dipole matrix elements as a consequence. The application of RLDI is restricted, however, to the study of species for which sufficiently high atomic-vapor densities can be achieved and the extension to high members of an isoelectronic sequence is limited by the need to provide dye lasers tuned to resonance transitions of ions for which the appropriate wavelengths move rapidly into the UV. It is not feasible therefore to study photoabsorption of either refractory metal vapors or ion stages greater than the second by the use of this method.

An alternative technique for recording photoabsorption spectra of ions is the dual laser plasma (DLP) method in which *both* the absorbing and back-lighting plasmas are produced by the interaction of high-power

laser beams with suitable solid targets. This method is not limited by the necessity to produce an atomic vapor in a heat pipe and has been consequently used to study a variety of atoms and ions. The first application by Carroll and Kennedy[31] was to Li^+ in the 60–250-eV region and enabled the two-electron excitations, $1s^2-2snp$ ^1P, to be studied. Tondello and co-workers in a series of experiments[32–37] studied photoabsorption in Be I–II, B II–IV, and C V. Using a synchronized twin-laser system and a time delay of the order of 1 μs between the generation of the absorbing plasma and that of the backlighting plasma, Carroll and Costello were able to observe the EUV photoabsorption spectra of the refractory elements Th and U for the first time.[38,39] More recently the DLP method was used by Brilly, Kennedy, and Mosnier[40] to study the sodium sequence up to the fourth stage of ionization. The versatility of the DLP is further illustrated by the work of Hansen et al.,[41] which extended the study of the Xe sequence to La^{3+}.

In the present work we report the $3p$ photoabsorption of Mn, Mn^+, Cr, and Cr^+ obtained using the DLP technique. We have previously studied $3p$ photoabsorption in Mn and Mn^+ using the RLDI method[42] and neutral chromium $3p$ photoabsorption has been previously studied by Sonntag and co-workers,[43] where chromium vapor produced in a heat pipe was backlighted by synchrotron radiation. We are now able to compare quantitatively the results obtained by the different techniques. This paper reports for the first time the $3p$ photoabsorption of Cr^+. The motivation for the study of $3p$ excitations in Cr^+ comes from two directions. In an earlier paper[42] $3p$ photoabsorption in neutral chromium was compared with that in its isoelectronic partner Mn^+ in an attempt to understand the strikingly intense series of Rydberg resonances converging to the $3p^53d^54s$ $^8P^\circ_{9/2,7/2,5/2}$ limits of Cr^+; the observed Rydberg series in Mn^+ is very much

weaker. We believe that the anomalous behavior of Cr is due to the location of the $3p^53d^64s$ $^7P^\circ$ resonance in the midst of the $3p^53d^54s(^8P^\circ)nl$ Rydberg region, to which it imparts some of its oscillator strength. To further check our understanding it is useful to study Cr^+ and the effect of the removal of a single valence $4s$ electron on $3p$ photoabsorption. The second motivating factor arises from a comparison of atomic, molecular, and solid-state EUV absorption involving manganese and chromium. In general terms, for manganese, a comparison of Mn, Mn^+, $MnCl_2$ (molecular), and $MnCl_2$ (solid) absorption shows that in the molecular and solid-state environments, atomic manganese effects are dominant. This is in sharp contrast to the case of chromium, where a comparison between Cr, $CrCl_2$ (molecular), and $CrCl_2$ (solid) absorption shows that atomic chromium excitations cannot account for the molecular or solid-state observations. It is of considerable interest therefore to observe the photoabsorption spectrum of Cr^+ to see if this provides an insight into the reasons for these differences.

EXPERIMENT

In the present work, the absorption spectra of Mn, Mn^+, Cr, and Cr^+ have been measured in the 47–69 and 38–63-eV regions. These results were obtained using the dual laser plasma technique; the absorbing column was created by ablation of spectroscopically pure manganese or chromium solid targets by a flash lamp pumped dye (Rhod 590) laser ($\sim$1 J in 1 μs and focal spot diameter $\sim$1 mm) and was back-lighted by an EUV continuum-emitting plasma created by a synchronized Nd:YAG (Nd-doped yttrium aluminum garnet) laser ($\sim$0.4 J in $\sim$20 ns with a focal spot diameter $\leq$100 μm). A schematic diagram of the experimental layout is shown in Fig. 1. Detection was via a self-scanning diode array in a
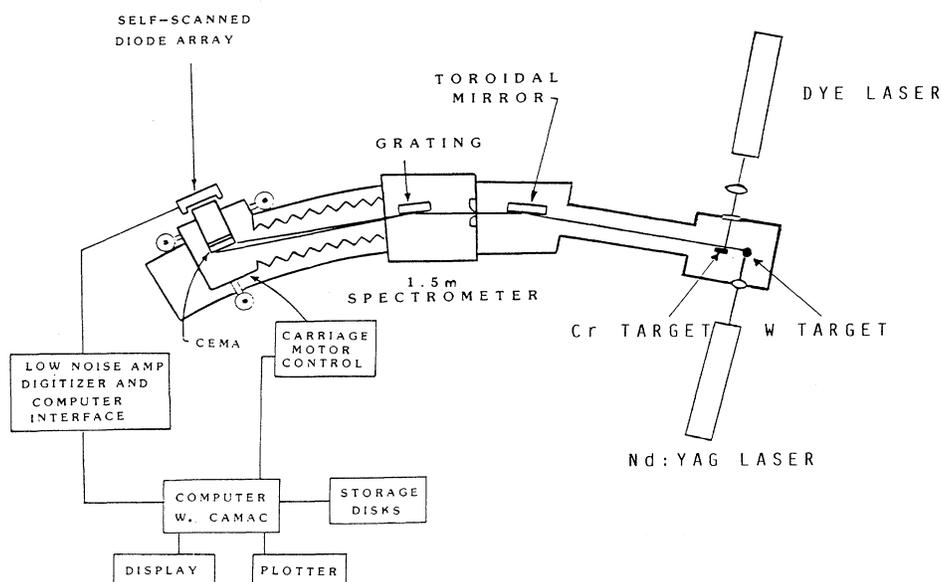
FIG. 1. Schematic representation of the experimental setup used for the dual laser plasma studies.

1.5-m grazing incidence spectrometer that has been described elsewhere[44]; the measured spectral resolution was ~2000 at 50 eV. The long pulse duration of the dye laser yielded a relatively cool manganese or chromium plasma at the beam focus. By adjusting the time delay between the Nd:YAG and dye laser pulses we were able to easily separate Mn,Mn⁺ and Cr,Cr⁺ photoabsorption spectra. The use of the long pulse duration (~ 1 μs) dye laser to create the absorbing plasma contrasts with earlier DLP work in which Q-switched laser pulses (~ 20–30 ns pulse widths) were exclusively used to produce the absorbing plasmas. To obtain strong absorption it was found necessary to ensure that the back-lighting continuum radiation passed by the manganese (or chromium) target less than 1 mm from the target surface. The estimated absorption column length was ~2 mm. Either tungsten or tantalum targets were used to produce the EUV continuum emitting plasma. The majority of spectra were recorded with a W background and the Ta was used to eliminate misinterpretation of weak spectral absorption features, which could arise from shot-to-shot variations in the background continuum. Energy calibration was achieved by recording emission spectra of plasmas formed by Nd:YAG-laser irradiation of aluminum targets. Internal calibration checks were carried out by comparing our measured energies of sharp absorption features in Mn, Mn⁺, and atomic chromium with those previously measured.

In order to obtain relative cross sections the following procedure was adopted. Spectra were recorded (and stored on the computer) both with (I) and without (I_0) the absorbing plasma. In order to reduce the influence of changes with time I and I_0 were recorded alternatively and the ratio I/I_0 for each pair was checked individually. In general, noise reduction was achieved by averaging the results of about 30 shots per spectral region (~ 5 eV wide). The logarithm of the ratio (I_0/I) was then taken to obtain the absorption spectra reported here. Results of overlapping spectral ranges were matched to obtain relative cross sections over the entire range covered. While the final spectra were obtained by averaging, it is important to note that every shot was monitored. Spectra with extreme variations which could be traced to either laser failure or poor target surfaces, were discarded. It was found necessary to preclean the manganese or chromium target surfaces by two or three preshots before commencing a series of photoabsorption measurements.

3p ABSORPTION OF FREE Cr, Cr⁺, Mn AND Mn⁺

Experimental results

We show in Fig. 2 absorption spectra of neutral and singly ionized manganese. Separation between Mn and Mn⁺ was achieved by shortening the time delay between the Nd:YAG and dye laser pulses from 3.3 to 1.3 μs. In earlier work we recorded Mn and Mn⁺ spectra using the RLDI technique. Figure 3 shows a comparison between the present results for Mn⁺ in the 58–69-eV region and those obtained earlier with RLDI. A detailed comparison of the Mn and Mn⁺ data over the 47–69-eV range
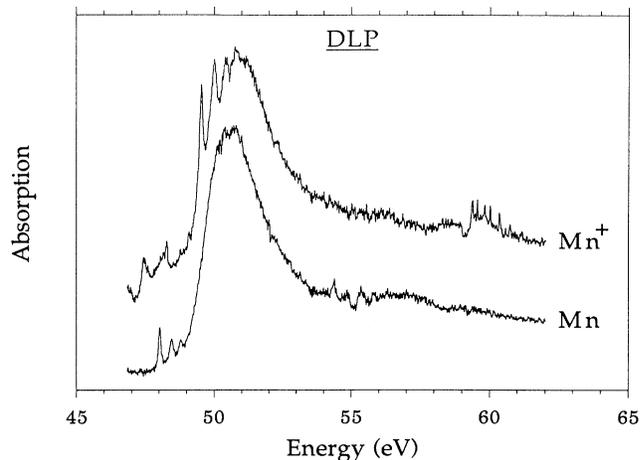
FIG. 2. Absorption spectra of neutral and singly ionized Mn. The amplitudes of the dominant $3p \rightarrow 3d$ resonances have been normalized.

shows that the DLP data are in very good agreement with the earlier RLDI data. For neutral Mn the present data could also be compared with results achieved using heat-pipe-generated vapors back-lighted by synchrotron radiation.[45] Again, very good agreement exists.

As stated earlier, the primary purpose of the present experiments was to record the Cr⁺ photoabsorption spectrum. Stimulated by our success in separating Mn and Mn⁺ we recorded the absorption of a chromium plasma versus time delay. The results shown in Fig. 4 demonstrate that shortening the time delay to less than 1.3 μs eliminates neutral chromium absorption. Figure 5 shows spectra recorded with time delays of 2.5 and 1.1 μs, respectively; an enlargement of the 1.1-μs data in the
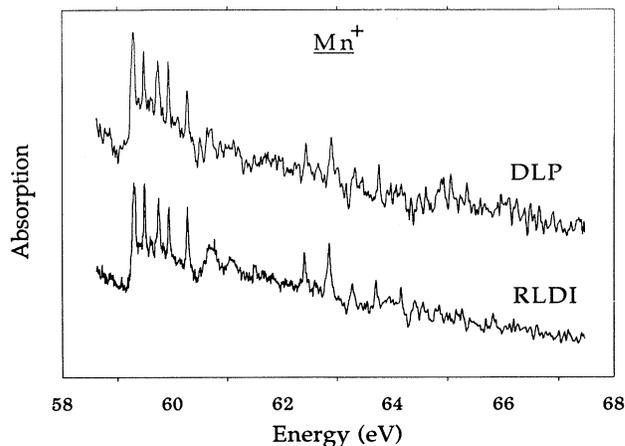
FIG. 3. Comparison between the Mn⁺ absorption spectra in the range of the $3p \rightarrow nl$ Rydberg series obtained by the resonant laser-driven ionization (RLDI) and the dual plasma technique (DLP). The amplitudes of the lowest energy $3p \rightarrow 5s$ Rydberg lines have been matched in height.

COSTELLO, KENNEDY, SONNTAG, AND CLARK
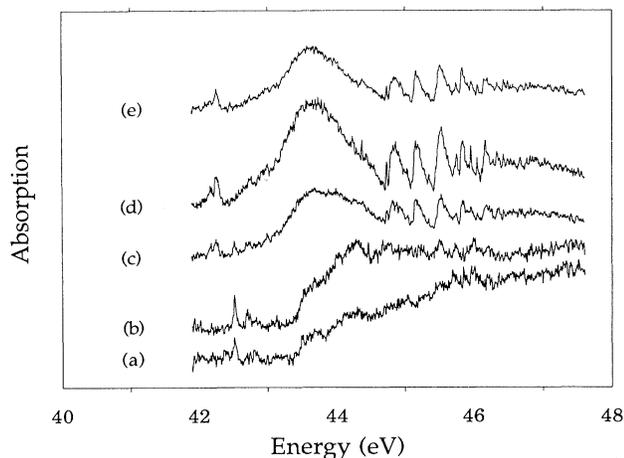
FIG. 4. 3p-absorption spectra of laser-produced Cr vapor taken at different time delays between the dye laser and Nd:Yag laser. [Time delays: curve (a) 0.8 μs, curve (b) 1.2 μs, curve (c) 1.6 μs, curve (d) 2.3 μs, and curve (e) 3.0 μs.]
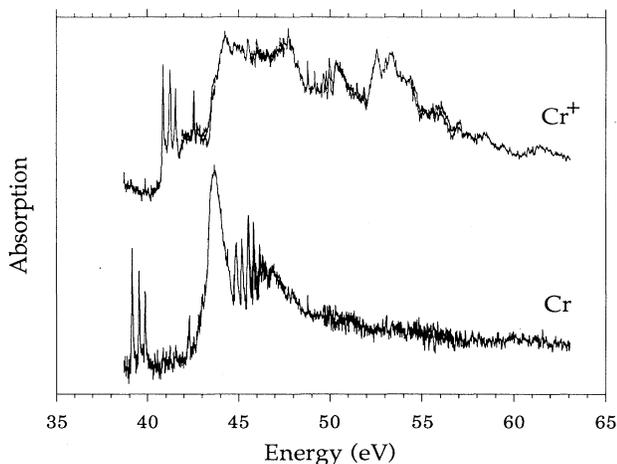
FIG. 5. Absorption spectra of Cr and Cr^+ recorded with time delays of 2.5 and 1.1 μs, respectively. The amplitudes of the lowest energy $3p \rightarrow 4s$ lines have been matched.
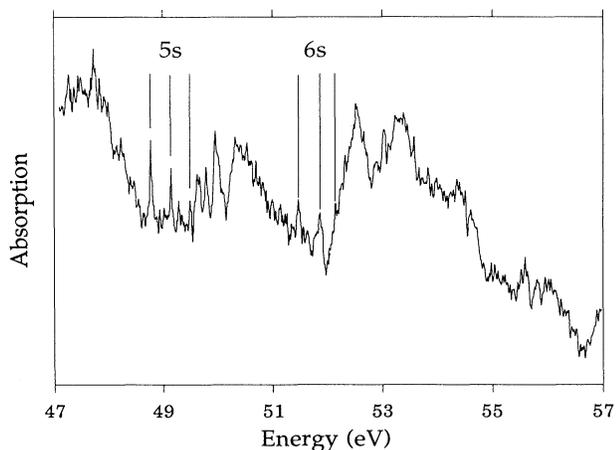
FIG. 6. Absorption spectrum of Cr^+ taken at a 1.1-μs time delay in the range of the $3p \rightarrow nl$ Rydberg transitions.
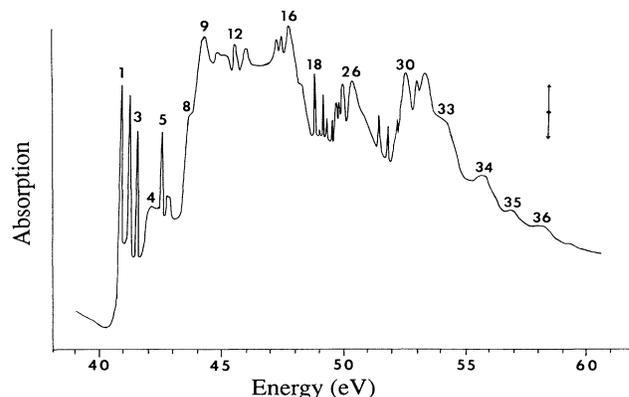
FIG. 7. Absorption spectrum of Cr^+ obtained by averaging over all experimental data taken at a 1.1-μs time delay. The error bar shows the estimated uncertainty in joining spectra in different energy ranges at regions of overlap.

46–57-eV region is shown in Fig. 6. The Cr^+ $3p$ absorption spectrum obtained by averaging over all experimental data is presented in Fig. 7. Taking into account experimental errors we estimate the uncertainty in the consistency of absorption spectra acquired in different spectral regions to be as indicated in Fig. 7. The observed neutral Cr data agree very well with the earlier photoelectric work of Meyer et al.[45] Table I contains a listing of the discrete features, observed in the 1.1-μs delayed spectrum, which are numbered in Fig. 7. The spectroscopic assignment in this table are based on atomic-structure calculations, which are described below.

DISCUSSION

The dominant feature in the $3p$ absorption spectra of all transition metals, whether as free atoms or bound atoms in molecules or solids, is the $3p \rightarrow 3d$ giant resonance. The essential nature of this resonance was first discussed by Dehmer et al.[46] and further elucidated by Davis and Feldkamp, who used a relatively simple model of a discrete $3p^5 3d^{n+1}$ state interacting with $3p^6 3d^{n-1}\epsilon f$ continua.[47] Subsequent ab initio calculations in a variety of approximations have confirmed the basic validity of this picture.[16,47–52]

The key aspects of the Davis-Feldkamp model may be summarized as follows. Although $3d$ electrons have binging energies typical of those of atomic valence electrons (< 10 eV), their spatial distribution resembles that of $3p$ electrons, which can be regarded as members of an inner shell (binding energy ~ 50 eV). The close overlap of the $3p$ and $3d$ orbitals results in a large dipole matrix element [the radial matrix element $(3p|r|3d) \approx 1$ a.u.], and this combines with the substantial excitation energy $\Delta E \approx 2$ a.u. to yield an oscillator strength $f \cong 2\Delta E |\langle 3p|r|3d \rangle|^2$ for the $3p \rightarrow 3d$ transition that is close to the number of electrons in the $3p$ shell. Since nd orbitals for $n > 3$ must be orthogonal to the $3d$ orbital, they correspondingly have small overlaps with the $3p$ orbital, and transitions between $3p$ and nd states are very

weak. The strength of $3p \rightarrow 4s$ transitions is comparable to that in elements on either side of the iron period (e.g., Ar, K, and Cu), for which $f = 0.1$; transitions to higher s states fall off in the fashion typical of Rydberg series. Thus almost all of the $3p$ absorption strength is associated with $3p \rightarrow 3d$ excitation. Since LS coupling is a fairly good approximation in the iron group, the spectrum is dominated by transitions to the relatively small number of final states that have the same (typically high) spin as the ground state.

The $3p \rightarrow 3d$ spin-allowed transitions are quite broad, with widths up to the order of several eV, and they show pronounced asymmetries. The large width derives from a dipole interaction of the $3p^5 3d^{n+1}$ states with $3p^6 3d^{n-1} \epsilon f$ continua, leading to autoionization. The

asymmetries of these peaks are enhanced by the relatively high oscillator-strength density associated with direct $3p^6 3d^n \rightarrow 3p^6 3d^{n-1} \epsilon f$ photoionization. Direct $3d \rightarrow \epsilon f$ excitation exhibits a delayed onset in this part of the Periodic Table, and the overlap of the continuum f wave with the M shell is largest at the electron energies at which $3d$ autoionization occurs (20–50 eV). The $3p \rightarrow 3d$ autoionization and $3d \rightarrow \epsilon f$ direct ionization amplitudes thus interfere and yield an asymmetric absorption profile.

The general ideas stated above appear to apply to most of the iron-group elements, and they have made possible reasonably good quantitative interpretation of the $3p$ absorption spectra in the framework of a Hartree-Fock description of the $3p^5 3d^{n+1}$ configuration, which autoionizes through interaction with the $3p^6 3d^{n-1} \epsilon f$ con-

TABLE I. Energies and assignments of observed features in the absorption spectrum of Cr$^+$. The uncertainty of the experimental energies is ± 0.05 eV for the sharp lines and ± 0.1 eV for the broader maxima.

Feature No.	Energy (eV)	Assignment	Calculated energy (eV)
1	40.90	$3p^5(^2P^\circ)3d^5(^6S)(^6P^\circ)4s\ ^6P^\circ_{7/2}$	41.02
2	41.28	$3p^5(^2P^\circ)3d^5(^6S)(^6P^\circ)4s\ ^6P^\circ_{5/2}$	41.39
3	41.58	$3p^5(^2P^\circ)3d^5(^6S)(^6P^\circ)4s\ ^6P^\circ_{3/2}$	41.68
4	41.98	$3p^5(^2P^\circ)3d^6(^5D)^6F^\circ_{7/2,5/2,3/2}$	42.9–43.2
5	42.59	$3p^5(^2P^\circ)3d^6(^5D)^6D^\circ_{5/2,3/2,7/2}$	43.9
		$3p^5(^2P^\circ)3d^5(^4D)(^5P^\circ)4s\ ^6P^\circ_{3/2}$	42.73
6	42.75	$3p^5(^2P^\circ)3d^5(^4D)(^5P^\circ)4s\ ^6P^\circ_{5/2}$	42.86
7	42.88	$3p^5(^2P^\circ)3d^5(^4D)(^5P^\circ)4s\ ^6P^\circ_{7/2}$	43.05
8	43.78	$3p^5(^2P^\circ)3d^6(^5D)^4P^\circ_{5/3,3/2}$	44.2–44.5
9	44.29	$3p^5(^2P^\circ)3d^6(^5D)^6P^\circ$	47.5–47.8
10	44.79		
11	45.24		
12	45.55	$3p^5(^2P^\circ)3d^5(^4P)(^5P^\circ)4s\ ^6P^\circ_{7/2}?$	46.63
13	46.02	$3p^5(^2P^\circ)3d^5(^4P)(^5P^\circ)4s\ ^6P^\circ_{5/3,3/2}?$	46.9
14	47.29		
15	47.48		
16	47.74		
17	48.24		
18	48.78	$3p^5(^2P^\circ)3d^5(^6S)(^7P^\circ)5s\ ^6P^\circ_{7/2}$	48.69
19	48.94	$3p^5(^2P^\circ)3d^5(^6S)(^7P^\circ)5s\ ^8P^\circ_{7/2}$	48.85
20	49.14	$3p^5(^2P^\circ)3d^5(^6S)(^7P^\circ)5s\ ^6P^\circ_{5/2}$	49.05
21	49.27	$3p^5(^2P^\circ)3d^5(^6S)(^7P^\circ)5s\ ^8P^\circ_{5/2}$	49.18
22	49.48	$3p^5(^2P^\circ)3d^5(^6S)(^7P^\circ)5s\ ^6P^\circ_{3/2}$	49.40
23	49.63		
24	49.76		
25	49.96		
26	50.36		
27	51.44		
		$3p^5(^2P^\circ)3d^5(^6S)(^7P^\circ)6s\ ^6P^\circ_{7/2}$	51.33
		$3p^5(^2P^\circ)3d^5(^4D)(^5P^\circ)5s\ ^6P^\circ_{3/2}$	51.43
		$3p^5(^2P^\circ)3d^5(^4D)(^5P^\circ)5s\ ^6P^\circ_{5/2}$	51.57
28	51.84		
		$3p^5(^2P^\circ)3d^5(^6S)(^7P^\circ)6s\ ^6P^\circ_{5/2}$	51.70
		$3p^5(^2P^\circ)3d^5(^4D)(^5P^\circ)5s\ ^6P^\circ_{7/2}$	51.76
29	52.16		
		$3p^5(^2P^\circ)3d^5(^6S)(^7P^\circ)6s\ ^6P^\circ_{3/2}$	52.02
30	52.54		
31	53.06		
32	53.32		
33	54.37		
34	55.8		
35	57.0		
36	58.4		

tinuum. However, this picture fails to account for a striking feature of the $3p$ absorption spectrum of Cr: significant oscillator strength in the nd Rydberg series, as seen between 45 and 47 eV in Figs. 4 and 5. Calculations at the Hartree-Fock level show no significant differences between Cr and Mn for the $3p \rightarrow nd$ dipole matrix elements nor for the matrix elements that couple $3p^5 3d^5 nd$ ($4s$ or $4s^2$) discrete states to the $3p^6 3d^4 \epsilon f$ ($4s$ or $4s^2$) continuum. It is apparent from Fig. 2 that the spectrum of isoelectronic Mn^+ $3p^6 3d^5(^6S)4s\,^7S$ fits the usual pattern of $3p$ absorption, so that the anomalous behavior of Cr is not solely due to the presence of an unpaired $4s$ electron in the ground state. We now describe a simple picture that shows why Cr and Mn^+ should be much different.

Figure 8 shows the level structure of the relevant $3p^5 3d^6 4s$ and $3p^5 3d^5 4d 4s$ states of Mn^+ and Cr (and the analogous $3p^5 3d^6$ and $3p^5 3d^5 4d$ states of Cr^+, which will be discussed below), as computed in the Hartree-Fock approximation, and referenced to the lowest $3p$ ionization limit (i.e., $3p^5 3d^5 4s\,^8P^\circ$ for Mn^+ and Cr, and $3p^5 3d^5\,^7P^\circ$ for Cr^+). Mn^+ exhibits conventional level ordering, in which $3p^5(^2P^\circ)3d^6(^5D)(^6P^\circ)4s\,^7P^\circ$ lies below $3p^5(^2P^\circ)3d^5(^6S)(^7P^\circ)4s(^8P^\circ)4d$ (and thus below all higher
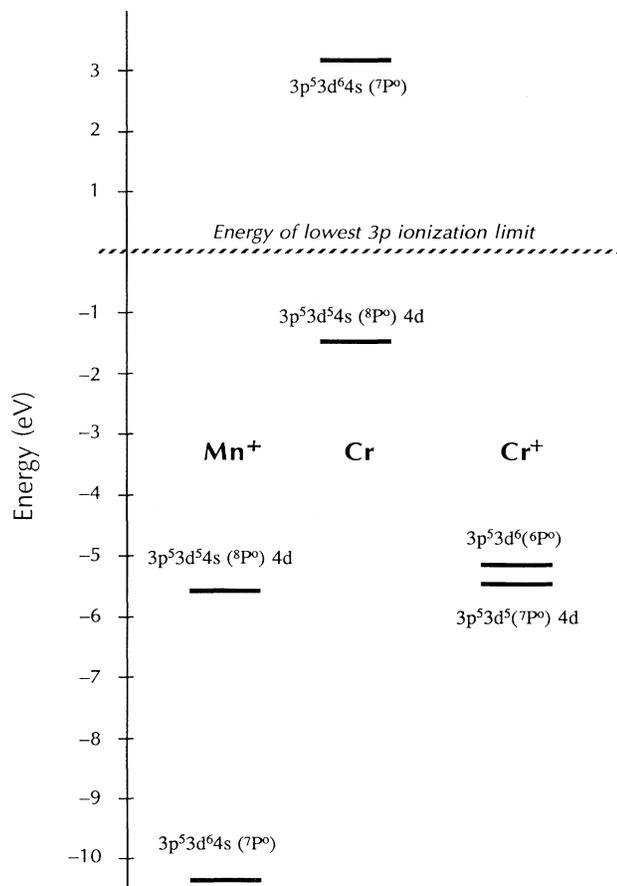
FIG. 8. Level structure of the $3p^5 3d^6 4s$ and $3p^5 3d^5 4d 4s$ states of Mn^+ and Cr and the analogous $3p^5 3d^6$ and $3p^5 3d^5 4d$ states of Cr^+ computed in the Hartree-Fock approximation. The levels are referenced to the lowest $3p$ ionization limit, i.e., $3p^5 3d^5 4s\,^8P^\circ$ for Mn^+ and Cr and $3p^5 3d^5\,^7P^\circ$ for Cr^+.

Rydberg states), as one would expect. The interaction of these states with the $3p^6 3d^{n-1} \epsilon f 4s$ continuum will thus result in the $3p^5 3d^6 4s$ state being broadened and shifted downward by several eV, and the $3p^5 3d^5 nd 4s$ states being relatively unchanged. Cr, on the other hand, has a level structure which at first glance seems inconsistent, in that $3p^5(^2P^\circ)3d^6(^5D)(^6P^\circ)4s\,^7P^\circ$ lies above the $3p^5(^2P^\circ)3d^5(^6S)(^7P^\circ)4s\,^8P^\circ$ ionization limit, and thus is above all members of the $3p^5(^2P^\circ)3d^5(^6S)(^7P^\circ)4s(^8P^\circ)nd$ Rydberg series. This apparent contradiction is resolved by noting that $3p^5(^2P^\circ)3d^6(^5D)(^6P^\circ)4s\,^7P^\circ$ is indeed bound with respect to the $3p^5(^2P^\circ)3d^5(^6S)(^5P^\circ)4s\,^6P^\circ$ limit, which lies 15 eV above the $^8P^\circ$ limit (in the subsequent discussion we drop the specific coupling notation for these states). The large energy difference between these limits derives from the exchange energy of $3p$ and $3d$ subshell interaction: the exchange integrals $G^1(3p, 3d)$ and $G^3(3p, 3d)$ are of the order of 10 eV, and have extremal weightings in the energy expression when all $3d$ spins are parallel [$3p^5(^2P^\circ)3d^5(^6S)(^7P^\circ)$] or antiparallel [$3p^5(^2P^\circ)3d^5(^6S)(^5P^\circ)$] to the $3p$ spin. Thus it happens that the $3p$-$3d$ exchange energy is significantly larger than the $3d$ ionization energy, and so the $3p^5 3d^6 4s\,^7P^\circ$ state, the symmetry of which requires having some $3p^5 3d^5 4s\,^6P^\circ$ parentage, can indeed lie above its other parent, $3p^5 3d^5 4s\,^8P^\circ$. Interaction with the $3p^6 3d^4 \epsilon f 4s$ continuum depresses the energy of the $3p^5 3d^6 4s\,^7P^\circ$ state, pushing it down into the region of the $3p^5 3d^5 nd 4s$ Rydberg series. The $3d^5 nd$ Rydberg states thus acquire their oscillator strengths and widths from interaction with the $3d^6$ resonance.

The mechanism has yet to be illustrated in an *ab initio* calculation, and we have not undertaken to perform one here. Our quantitative theoretical analysis is confined to states whose properties are not dominated by interaction with the autoionization continuum. However, it is worth noting what the above picture implies for the $3p$ absorption spectrum of Cr^+. The rightmost region of Fig. 8 shows the analogous portion of its level scheme. Due to the increase of the ionization potential, the $3p^5 3d^6\,^6P^\circ$ state now lies *below* the $3p^5 3d^5\,^7P^\circ$ limit, but it lies very close to the $3p^5 3d^5 4d\,^6P^\circ$ state. When these two states are allowed to interact in the multiconfiguration Hartree-Fock approximation, the resulting eigenstates consist of nearly equal admixtures, though the coefficients are sensitive to the zeroth-order difference in energy between the two configurations. Thus there is strong configuration interaction between $3p^5 3d^6\,^6P^\circ$ and the $3p^5 3d^5 nd\,^6P^\circ$ Rydberg series in addition to the interaction with the f-wave continuum. We presume that this is the mechanism that produces the diffuse structure observed in the absorption spectrum of Cr^+ by distributing the $3p \rightarrow 3d$ oscillator strength among several Rydberg states.

We have carried out calculations of atomic-energy levels and transition probabilities at several levels of approximation, using both a standard multiconfigurational Hartree-Fock approximation[53] and Cowan's general atomic structure code.[54] These approaches lead to good quantitative results for excited states of the $3p^5 3d^5 4s^q ns$ configurations, and they enable us to determine the $3p$

ionization limits with reasonable accuracy. For Mn and Mn$^+$ our results also appear to give a reasonable account of $3p^5 3d^5 4s^q 4d$ states, which have very small oscillator strengths and widths. Results for Mn and Mn$^+$ have been reported in previous work[42] and we have no significant revisions to make to the previous classification[43] of the Cr spectrum. We focus here on Cr$^+$. The key results of these calculations are summarized in Table I, which we now discuss.

The three strong lines around 41 eV are undoubtedly the expected $3p^6 3d^5 \, ^6S_{5/2} \rightarrow 3p^5 3d^5 4s \, ^6P^\circ_{3/2,5/2,7/2}$ triplet. The agreement of the observed and calculated energies to within 0.1 eV is fortuitous, since analogous calculations for the Cr $3p^5 3d^5 4s^2$ states deviate by 0.5 eV from observations; however, the agreement of the relative positions is comparable in both cases. By adding the 6.7667-eV ionization potential[55] of Cr to these energies, we obtain values of the $3p^5 3d^5 4s \, ^6P^\circ$ ionization limits of Cr: 47.67, 48.05, and 48.35 eV. The oscillator strengths of transitions to $3p^5 3d^5 4s \, ^8P^\circ$ states are about 1% of those to $^6P^\circ$ states, and we cannot see them with any certainty in our spectrum. By referencing our calculated energies of the octet states to the experimental values of the sextets, we would place $3p^5 3d^5 4s \, ^8P^\circ_{5/2,7/2}$ at 40.21 and 39.90 eV, respectively. These would correspond to $3p$ ionization limits of Cr of 46.97 and 46.67 eV, respectively; these are to be compared with the limits of 47.050 and 46.725 eV (± 0.01 eV) previously inferred[43] from quantum-defect analysis of the ns and nd Rydberg series of Cr. That analysis classified all states in terms of $^8P^\circ$ limits; since we now know that the $^6P^\circ_{7/2}$ limit lies only 0.6 eV above $^8P^\circ_{5/2}$, it probably should be included in any more detailed analyses.

Identification of the intercombination transitions to $3p^5 3d^6 \, ^6F^\circ$, $^6D^\circ$, and $^4P^\circ$ states is largely based on analogy with previous classifications of the spectra of Mn, Mn$^+$, and Cr. All of these states have very low oscillator strengths in the present calculation, but this is presumably because the $^6P^\circ$ states from which they obtain their intensities are placed too high.

The appearance of $3p^5(^2P^\circ)3d^5(^4D)(^5P^\circ)4s \, ^6P^\circ$ states at 42.8 eV and $3p^5(^2P^\circ)3d^5(^4P)(^5P^\circ)4s \, ^6P^\circ$ states at 45.5–46 eV illustrates a phenomenon that has not previously been encountered in $3p \rightarrow 4s$ excitation in this region of the Periodic Table: the existence of states that interact with the $3d^5 \, ^6S$ core term in LS coupling, without the aid of spin-orbit interaction. This may also occur in $5s$ excitation: features 27–29 could be associated with $3p^5(^2P^\circ)3d^5(^4D)(^5P^\circ)5s \, ^6P^\circ$ states, though $3p^5(^2P^\circ)3d^5(^6S)(^7P^\circ)6s \, ^6P^\circ$ states occur in the same energy region and with similar oscillator strengths.

The calculated energies of the $3p^5 3d^6 \, ^6P^\circ$ states are too high by about 3.5 eV; a compensating shift due to interaction with the f-wave continuum is not unreasonable. Feature No. 16 is conceivably a $3p^5 3d^5 4d$ state with a substantial admixture of $3p^5 3d^6$.

Identification of the $5s$ states (features 18–22) is fairly unambiguous. We use the $4s$ and $5s$ levels to estimate the ionization limits as follows. It has been found that the quantum defects of Rydberg electrons bound to core-excited atoms are very close to the quantum defects of isoionic Rydberg states built on closed shells, and that the differences in quantum defects is given fairly accurately by Hartree-Fock calculations. In particular, we would expect the quantum defects of Cr$^+$ $3p^5 3d^5(^6S)ns$ to be close to those of Mn$^+$ $3p^6 3d^5(^6S)ns$; the latter can be determined from optical data.[56] We add the correction inferred from the Mn$^+$ spectra to the Cr$^+$ quantum defect to obtain an estimate of the experimental value as follows.

State	Hartree-Fock	Quantum-defect experiment	Correction
Mn$^+$ $3d^5(^6S)4s \, ^5S$	1.986	2.060	0.074
Cr$^+$ $(3p^5(^2P^\circ)3d^5(^6S)(^6P^\circ)4s \, ^6P^\circ$	1.948	(2.022)	
Mn$^+$ $3d^5(^6S)5s \, ^5S$	1.965	2.030	0.065
Cr$^+$ $3p^5(^2P^\circ)3d^5(^6S)(^6P^\circ)5s \, ^6P^\circ$	1.927	(1.992)	
Mn$^+$ $3d^5(^6S)6s \, ^5S$	1.958	2.022	0.064
Cr$^+$ $3p^5(^2P^\circ)3d^5(^6S)(^6P^\circ)6s \, ^6P^\circ$	1.920	(1.984)	

By assuming these estimates to apply to the centers of gravity of the $4s$ and $5s \, ^6P^\circ$ terms in whose identification we are reasonably confident, we find a mean ionization potential (averaged over $3p^5 3d^5 \, ^7P^\circ$ fine structure) of 55.09 eV from the $4s$ configuration, and 55.07 eV from the $5s$. By further assuming that the fine structure of Cr^{2+} $3p^5 3d^5 \, ^7P^\circ$ is the same as that of Cr $3p^5 3d^5 4s^2 \, ^7P^\circ$, we get the following limit structure: $3p^5 3d^5 \, ^7P^\circ_4 = 54.8$ eV, $^7P^\circ_3 = 55.2$ eV, and $^7P^\circ_2 = 55.5$ eV. The calculated $6s$ energies give limits that agree well with these values. A direct quantum-defect analysis of the observed ns series provides values which agree with these limits, apart from the $^7P^\circ_2$ limit for which a value of 55.3 eV is obtained.

With these limits, feature No. 16 is found to have a quantum defect of 1.3–1.4, which is larger than normal for the $4d$ state in this region (0.7–1.0). The group of features 23–26 has quantum defects that are roughly normal for a $4d$ state. The next clump of broad features (30–32) does not appear to have energies that are consistent with a $3p^5 3d^5(^7P^\circ)nd$ state. Thus the assignment of the major broad structures in the Cr$^+$ absorption spectrum must be left to future work.

As a footnote to the previous work[42] we provide an application of the analysis discussed above to the identification of Rydberg features in the $3p$ absorption spectrum of Mn. Identification of the $3p^5 3d^5 4s^2 \, ^7P^\circ_{4,3,2}$ states in photoabsorption by Mn$^+$ (visible as a triplet on the shoulder of the giant resonance in Fig. 2) makes possible the assignment of the weak features observed in neutral Mn at around 55 eV, since these states define the lim-

its to which the Mn Rydberg series $3p^53d^54s^2nl$ converge. The quantum defects of the ns and nd series members are estimated as above for the isoionic pair Mn $3p^53d^54s^2nl$ and Mn $3p^63d^54snl$. The latter values can be compared with existing spectroscopic data, and the

differences between experimental and computed values $(\Delta\mu \sim 0.08)$ are then used as a correction to the Hartree-Fock quantum defect of the corresponding core-excited state. The main features in Mn $3p$ absorption may then be classified.

Energy (eV)	Designation	Quantum defect with respect to parent state	
		Calculated	Observed
54.50	$3p^5(^2P^\circ)3d^5(^6S)4s^2(^7P^\circ_4)5s\,^6P^\circ_{7/2}$	2.696	2.705
54.85	$3p^5(^2P^\circ)3d^5(^6S)4s^2(^7P^\circ_3)5s\,^6P^\circ$	2.696	2.719
55.36	$3p^5(^2P^\circ)3d^5(^6S)4s^2(^7P^\circ_2)5s\,^6P^\circ$	2.696	2.678
	$3p^5(^2P^\circ)3d^5(^6S)4s^2(^7P^\circ_4)4d\,^6P^\circ$	1.129	1.106
55.78	$3p^5(^2P^\circ)3d^5(^6S)4s^2(^7P^\circ_4)6s\,^6P^\circ$	2.662	2.639
	$3p^5(^2P^\circ)3d^5(^6S)4s^2(^7P^\circ_3)4d\,^6P^\circ$	1.129	1.158

Assignment of the lowest two features on this basis seems unambiguous. The features at 55.36 and 55.78 eV may be composites of s and d states, but the larger oscillator strength of the s series would tend to imply that the main features are s states. These identifications appear to be consistent with the results of photoelectron spectra.[56]

3p ABSORPTION OF Mn AND Cr METAL, AND MOLECULAR AND SOLID $MnCl_2$ AND $CrCl_2$

Due to the local character of final-state orbitals, atomic effects often dominate the inner-shell spectra of molecules and solids. The strong atomic $3p^63d^n \rightarrow 3p^53d^{n+1}$ autoionizing resonances are well preserved in the $3p$ absorption spectra of the $3d$ transition metals Mn, Fe, Co, and Ni[45,57,58] and their halides.[12,13,16,59] The asymmetric Fano-type line shape[60] caused by the interference between the $3p^63d^n \rightarrow 3p^53d^{n+1}$ and the $3d^n \rightarrow 3d^{n-1}\epsilon f$ excitation is also displayed by the partial photoelectron yield spectra of these metals and the corresponding metal halides.[14-16,45,61-63] The $3p$-absorption spectra of Mn metal,[64] Mn atoms,[45] Mn^+ ions,[42] molecular $MnCl_2$,[65] and solid $MnCl_2$ (Refs. 14 and 59) are shown in Fig. 9. In respect to energy position, relative strength, and shape, there is a close similarity between the dominant maxima in the spectra of atomic Mn, molecular $MnCl_2$ and solid $MnCl_2$. This demonstrates that for the giant resonance the intra-atomic interactions prevail over the influence of the ligands. This is corroborated by the similarity of the spectra of the linear $MnCl_2$ molecule and the cubic $MnCl_2$ solid. The Mn^+ ion displays a broader resonance on which the $3p^63d^54s\,^7S_3 \rightarrow 3p^53d^54s^2\,^7P_{2,3,4}$ lines are superimposed on the low-energy side. In this respect, the Mn^+ spectrum markedly differs from that of the Mn chlorides. There is also a strong asymmetric resonance in the spectrum of Mn metal which resembles the Mn^+ spectrum if one allows for a solid-state broadening. Shin et al.[59] could quite well reproduce the experimental $3p$-absorption spectrum of solid $MnCl_2$ by model calculations based on (i) the multiplet splitting of the Mn^{2+} $3P^63d^5 \rightarrow 3p^53d^6$ excitations, (ii) the influence of the field at the Mn^{2+} site created by the Cl^- ligands, and (iii) the

Fano-type line shape due to the interference between the $3p^63d^5 \rightarrow 3p^53d^6$ and the $3d^5 \rightarrow 3d^4\epsilon f$ excitations. But the spectra given in Fig. 9 raise the question whether Mn^{2+} is the best starting point and whether the neglect of the $3p$-$4s$ transitions for Mn^{2+} is justified.

The $3p$ spectra of Cr do not fit into the series Mn through Ni. The Cr atom is the only member of the $3d$ metal group that displays a set of well-developed Rydberg series converging towards the Cr^+ $3p^53d^54s\,^8P$ ionization limits.[43,45] Up to now no convincing explanation has been put forward for the broad, double-peaked structure encountered above the $3p$ absorption threshold of Cr
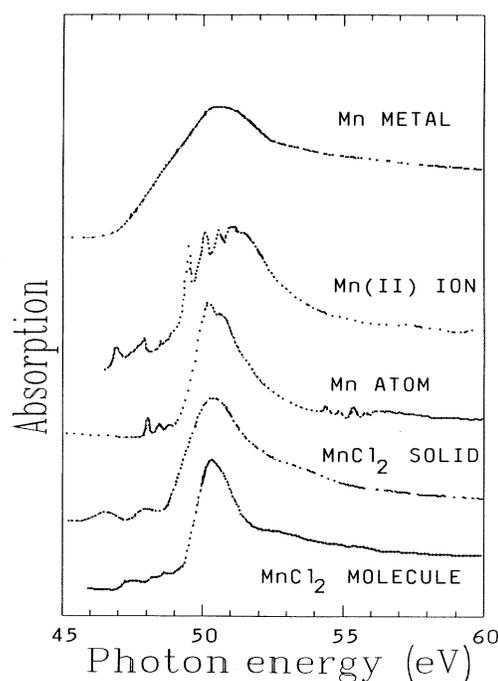
FIG. 9. Absorption spectra of Mn metal (Ref. 65), Mn atoms (Refs. 42 and 45), Mn^+ ions (Ref. 42), molecular (Ref. 56) and solid $MnCl_2$ (Ref. 14) in the range of the $3p$ excitations.

metal.[15,46,64] From the 3p-absorption spectra of atomic and metallic Cr presented in Fig. 10 it is obvious that an interpretation of the metal spectrum cannot be based on the atomic spectrum. For comparison the 3p absorption of Cr$^+$ ions, molecular CrCl$_2$ (Ref. 65), and solid CrCl$_2$ (Ref. 12) are included in Fig. 10. Note that Shin et al.[59] reported a spectrum of solid CrCl$_2$ which is considerably different from that of Nakai et al.[12] In both experiments the samples were evaporated in situ onto collodion films. The reason for the discrepancies may rest with different stoichiometry[59] or water of crystallization. The spectra of the molecular species represent the absorption of an approximately 50-cm-long vapor column maintained inside a resistivity heated tubular furnace (temperature MnCl$_2 \sim 600$ °C, CrCl$_2 \sim 700$ °C). In order to remove the water of crystallation, commercial salts were carefully outgassed at low temperatures, before taking the spectra.

The spectra of solid and molecular CrCl$_2$ presented in Fig. 10 closely resemble each other. In order to facilitate comparison to the molecular spectrum, the 3p absorption of solid CrCl$_2$ (Ref. 12) has been shifted towards lower photon energies by 2 eV. Both spectra bear no resemblance to the spectrum of atomic Cr. The most striking result presented in Fig. 10 is the close similarity of the spectra of the Cr halides with that of the Cr$^+$ ion. In all three spectra the absorption maxima at threshold can be ascribed to 3p-4s transitions, whereas 3p-nd transitions are responsible for the broad and structured absorption maximum extending 10 eV above threshold. Cr$^+$ intraionic interactions seem to determine the main features of the halide spectra. The influence of the ligands mainly results in a smearing of the Cr$^+$ fine structure. In light of these results the interpretation of the solid CrCl$_2$ spectrum based on the Cr^{2+} $3p^53d^4 \rightarrow 3p^53d^5$ excitations modified by the ligand field[13,59] has to be questioned. Especially the complete neglect of the 3p-4s transitions in these model calculations seems to be unjustified. The double hump and the width of the metal resonance reflect the Cr$^+$ spectrum. It is tempting to ascribe the main feature of the metal to localized Cr$^+$ 3p excitations broadened by the solid-state environment.
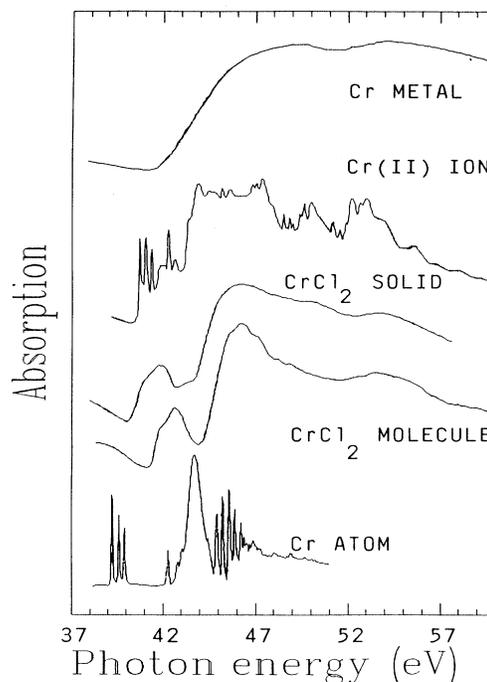
FIG. 10. Absorption spectra of Cr metal (Ref. 65), Cr atoms (Refs. 43 and 45), Cr$^+$ ions, molecular (Refs. 66) and solid (Ref. 12) CrCl$_2$ in the range of the 3p excitations. In order to facilitate comparison the spectrum of solid CrCl$_2$ has been shifted towards lower energies by 2 eV.

[1]P. S. Bagus, Phys. Rev. 139, A619 (1965).

[2]A. Msezane, R. F. Reilman, S. T. Manson, J. R. Swanson, and L. Armstrong, Jr., Phys. Rev. A 15, 668 (1977).

[3]W. Ong, S. T. Manson, A. K. Tseng, and R. H. Pratt, Phys. Lett. 69A, 319 (1979).

[4]R. F. Reilman and S. T. Manson, Astrophys. J. Suppl. Ser. 40, 815 (1979).

[5]K. D. Chao and S. T. Manson, Phys. Rev. A 24, 2481 (1981).

[6]K. T. Cheng and C. Froese Fischer, Phys. Rev. A 28, 2811 (1983).

[7]K. T. Cheng and W. R. Johnson, Phys. Rev. A 28, 2820 (1983).

[8]M. Ya. Amusia, V. K. Ivanov, and V. A. Kupchenko, J. Phys. B 18, 3871 (1985).

[9]R. D. Cowan and M. Wilson, J. Phys. B 21, L201 (1988).

[10]N. R. Simon, Astrophys. J. 260, L87 (1982).

[11]W. H. Parkinson, Spectroscopy of Astrophysical Plasmas, edited by A. Dalgarno and D. Layzer (Cambridge University Press, Cambridge, 1987), p. 302.

[12]S. Nakai, H. Nakamori, A. Tomita, K. Tsutsumi, H. Nakamura, and C. Sugiura, Phys. Rev. B 9, 1870 (1974).

[13]T. Yamaguchi, S. Shibuya, S. Suga, and S. Shin, J. Phys. C 15, 2641 (1982).

[14]A. Kakizaki, K. Sugeno, T. Ishii, H. Sugawara, I. Nagakura, and S. Shin, Phys. Rev. B 28, 1026 (1983).

[15]H. Sugawara, K. Naito, T. Miya, A. Kakizaki, I. Nagakura, and T. Ishii, J. Phys. Soc. Jpn. 53, 279 (1984).

[16]L. C. Davis, J. Appl. Phys. 59, R25 (1986).

[17]B. Hermsmeier, C. S. Fadley, M. O. Krause, J. Jimenez-Mier, P. Gerard, and S. T. Manson, Phys. Rev. Lett. 61, 2592 (1988).

[18]A. M. Cantu, W. H. Parkinson, G. Tondello, and G. P. Tozzi, J. Opt. Soc. Am. 67, 1030 (1977).

[19]G. Mehlman, G. Balloffet, and J. M. Esteva, Astrophys. J. **157**, 945 (1969).

[20]J. M. Esteva and G. Mehlman, Astrophys. J. **193**, 1 (1974).

[21]I. C. Lyon, B. Peart, J. B. West, and K. Dolder, J. Phys. B **19**, 4137 (1986); **20**, 1471 (1987).

[22]I. C. Lyon, B. Peart, and K. Dolder, J. Phys. B **20**, 1925 (1987); B. Peart and I. C. Lyon, *ibid.* **20**, L673 (1987).

[23]T. B. Lucatorto and T. J. McIlrath, Phys. Rev. Lett. **37**, 428 (1976).

[24]T. J. McIlrath and T. B. Lucartorto, Phys. Rev. Lett. **38**, 1390 (1977).

[25]T. B. Lucatorto and T. J. McIlrath, Appl. Opt. **19**, 3948 (1980).

[26]W. T. Hill, K. T. Cheng, W. R. Johnson, T. B. Lucatorto, T. J. McIlrath, and J. Sugar, Phys. Rev. Lett. **49**, 1631 (1982).

[27]B. F. Sonntag, C. L. Cromer, Y. M. Bridges, T. J. McIlrath, and T. B. Lucatorto, in *Short Wavelength Coherent Radiation: Generation and Applications (Monterey, California 1986),* Proceedings of the Topical Meeting on Short Wavelength Coherent Radiation, AIP Conf. Proc. No. 147, edited by D. T. Attwood and Y. Bokor (AIP, New York, 1986), p. 412.

[28]T. B. Lucatorto, T. J. McIlrath, J. Sugar, and S. M. Younger, Phys. Rev. Lett. **47**, 1124 (1981).

[29]C. W. Clark, J. Opt. Soc. Am. B **1**, 626 (1984).

[30]C. W. Clark and T. B. Lucatorto, in *Giant Resonances in Atoms, Molecules and Solids,* edited by J. P. Connerade, J. M. Esteva, and R. C. Karnatek, Vol. 151 of *NATO ASI, Series B: Physics* (Plenum, New York, 1987), p. 137.

[31]P. K. Carroll and E. T. Kennedy, Phys. Rev. Lett. **38**, 1068 (1977).

[32]E. Jannitti, P. Nicolosi, and G. Tondello, Physica **124C**, 139 (1984).

[33]E. Jannitti, M. Mazzoni, P. Nicolosi, G. Tondello, and W. Yongchang, J. Opt. Soc. Am. B **2**, 1078 (1985).

[34]E. Jannitti, F. Pinghong, and G. Tondello, Phys. Scr. **33**, 434 (1986).

[35]E. Jannitti, P. Nicolosi, and G. Tondello, Phys. Scr. **36**, 93 (1987).

[36]E. Jannitti, P. Nicolosi, and G. Tondello, Opt. Commun. **63**, 37 (1987).

[37]E. Jannitti, P. Nicolosi, and G. Tondello, Phys. Lett. **A131**, 186 (1988).

[38]P. K. Carroll and J. T. Costello, Phys. Rev. Lett. **57**, 1581 (1986).

[39]P. K. Carroll and J. T. Costello, J. Phys. **1320**, L207 (1987).

[40]J. Brilly, E. T. Kennedy, and J. P. Mosnier, J. Phys. B **21**, 3685 (1988).

[41]J. E. Hansen, J. Brilly, E. T. Kennedy, and G. O'Sullivan, Phys. Rev. Lett. **63**, 1934 (1989).

[42]J. W. Cooper, C. W. Clark, C. L. Cromer, T. B. Lucatorto, B. F. Sonntag, E. T. Kennedy, and J. T. Costello, Phys. Rev. A **39**, 6074 (1989).

[43]R. Bruhn, E. Schmidt, H. Schroder, and B. Sonntag, J. Phys. B **15**, 2807 (1982).

[44]C. L. Cromer, J. Bridges, and T. B. Lucatorto, Appl. Opt. **24**, 2996 (1985).

[45]M. Meyer, Th. Prescher, E. von Raven, M. Richter, E. Schmidt, B. F. Sonntag, and H. E. Wetzel, Z. Phys. D **2**, 347 (1986).

[46]J. L. Dehmer, A. F. Starace, U. Fano, J. Sugar, and J. W. Cooper, Phys. Rev. Lett. **26**, 1521 (1971).

[47]L. C. Davis and L. A. Feldkamp, Solid State Commun. **19**, 413 (1976); Phys. Rev. A **17**, 2012 (1978).

[48]L. J. Garvin, E. R. Brown, S. L. Carter, and H. P. Kelly, J. Phys. B **16**, L269 (1983); **16**, L643 (1983).

[49]J. Jimenez-Mier, M. O. Krause, P. Gerard, B. Hermsmeier, and C. S. Fadley, Phys. Rev. A **40**, 3712 (1989).

[50]F. Combet-Farnoux and M. BenAmar, Phys. Rev. A **21**, 1975 (1980).

[51]M. Ya. Amusia, V. K. Dolmatov, and V. K. Ivanov, J. Phys. B **16**, L753 (1983).

[52]M. Ya. Amusia, V. K. Dolmatov, and V. M. Romanenko, J. Phys. B **21**, L151 (1988).

[53]C. Froese Fischer, Comput. Phys. Commun. **14**, 145 (1978).

[54]R. Cowan, *Theory of Atomic Structure and Spectra* (University of California Press, Brekeley, 1981).

[55]J. Sugar and C. Corliss, J. Phys. Chem. Ref. Data **14**, Suppl. 2, 1 (1985).

[56]E. Schmidt, H. Schroder, B. Sonntag, H. Voss, and H. E. Wetzel, J. Phys. B **18**, 79 (1985).

[57]R. Bruhn, B. Sonntag, and H. W. Wolff, Phys. Lett. **69A**, 9 (1978).

[58]R. Bruhn, B. Sonntag, and H. W. Wolff, J. Phys. B **12**, 203 (1979).

[59]S. Shin, S. Suga, M. Taniguchi, H. Kanzaki, S. Shibuya, and T. Yamaguchi, J. Phys. Soc. Jpn. **51**, 906 (1982).

[60]U. Fano, Phys. Rev. **124**, 1866 (1961).

[61]D. Chandesris, J. Lecante, and Y. Petroff, Phys. Rev. B **27**, 2630 (1983).

[62]H. Sugawara, A. Kakizaki, I. Nagakura, and T. Ishii, J. Phys. F **12**, 2929 (1982).

[63]H. Kato, T. Ishii, S. Masuda, Y. Harada, T. Komeda, M. Onchi, and Y. Sakisaka, Phys. Rev. B **32**, 1992 (1985).

[64]B. Sonntag, R. Haensel, and C. Kunz, Solid State Commun. **7**, 597 (1969).

[65]M. Heymann, Diplomthesis, Universität Hamburg, 1988; DESY Internal Report No. F41 HASYLAB-88-01 (unpublished).